UHTC-carbon fibre composites

Paul, A.; Venugopal, S.; Binner, Jonathan; Vaidhyanathan, B.; Heaton, A. C J; Brown, P. M.

DOI:
10.1016/j.jeurceramsoc.2012.08.018

Document Version
Peer reviewed version

UHTC – Carbon Fiber Composites: Preparation, Oxyacetylene Torch Testing and Characterisation

A. Paul[a], S. Venugopal[a], J.G.P. Binner[a], B. Vaidhyanathan[a], A.C.J. Heaton[b] and P.M. Brown[b]

[a]Department of Materials, Loughborough University, UK, LE11 3TU

[b]DSTL, Porton Down, Salisbury, UK, SP4 0JQ

Abstract

Current generation carbon-carbon (C-C) and carbon-silicon carbide (C-SiC) materials are limited to service temperatures below 1800°C and materials are sought that can withstand higher temperatures and ablative conditions for aerospace applications. One potential materials solution is carbon fiber-based composites with matrices composed of one or more ultra high temperature ceramics (UHTCs); the latter are intended to protect the carbon fibers at high temperatures whilst the former provides increased toughness and thermal shock resistance to the system as a whole. Carbon fiber-UHTC powder composites have been prepared via a slurry impregnation and pyrolysis route. Five different UHTC compositions have been used for impregnation, viz. ZrB_2, ZrB_2-20 vol% SiC, ZrB_2-20 vol% SiC-10 vol% LaB_6, HfB_2 and HfC. Their high-temperature oxidation resistance has been studied using a purpose built oxyacetylene torch test facility at temperatures above 2500°C and the results are compared with that of a C-C

benchmark composite. [1]The oxidation products have been characterized using various techniques and the results show that hafnium diboride-based UHTC composites offered the greatest resistance to ultra high temperature oxidation.

Key words: Ultra high temperature, oxyacetylene torch testing, oxidation

Introduction

Refractory transition metal borides and carbides have extremely high melting points of over 3000°C and hence are referred to as ultra high temperature ceramics (UHTCs). Even though they have been studied since the1960s, there has been recent interest in these materials as potential candidates for thermal protection systems on hypersonic vehicles. A developmental history of UHTC materials can be found in Opeka et al.,[1] and they have recently been reviewed by Paul et al.[2] The initial selection of UHTC materials was based on their melting temperatures, however oxidation temperature and the melting points of their oxides is, in fact, more critical. There are a number of materials with melting points over 3000°C, whose oxides also have melting points in excess of 2500°C, for example ZrB_2, HfB_2 and HfC. These materials are widely studied for high temperature applications as monolithic components, however single phase ceramics are significantly limited in this area as a result of their very poor thermal shock and oxidation resistance.[3] Even with the addition of a second or third ceramic phase such as SiC or LaB_6, these materials do not possess the high temperature resistance, thermal shock resistance or fracture toughness because of the volatilization and decomposition of the oxidation products.[4]

The desired properties may require the development of fiber reinforced UHTC composites to enable viable application development beyond 2500°C. For such hybrid materials, carbon fiber is the preferred choice owing to its high strength, ready availability and ability to be formed into complex shapes,[5] *provided* it can be protected from oxidation.

There are a number reports in the literature describing the preparation of fiber reinforced composites for UHT applications, of which those developed by Levine et al.[6,7] are amongst the earliest. They studied the high temperature oxidation resistance of SiC fiber reinforced ZrB_2-20 vol% SiC, prepared via filament winding, slurry impregnation and hot pressing, against that of non-reinforced ZrB_2-20 vol% SiC at up to 1927°C for periods of up to 100 minutes.[6] Whilst the non-reinforced material showed the best oxidation protection at 1327°C and 1627°C, at 1927°C both compositions underwent severe degradation and bloating and the authors expressed concerns about the thermal shock resistance of the non-reinforced materials in high heat flux, aeroconvective environments. The same group[7] prepared UHTC composites using Zoltek Panex® 30 carbon fabric, allylhydridopolycarbosilane preceramic polymer, HfB_2 and SiC powders, to create a graded structure, from a HfB_2-rich surface through to a SiC-rich surface with Si-O-C pre-ceramic polymer throughout, although micro-cracks were present in the final composites. Oxidation testing was carried out in a furnace at 1617°C and using an oxyacetylene flame at 1805-2015°C. Following cyclic heating in the furnace, a non-uniform $HfSiO_4$ and monoclinic HfO_2 surface was formed on the HfB_2-rich surface and a

glassy SiO_2 layer was formed on the SiC-rich surface. Damage to the carbon fibers in the furnace testing was found to be lower at the HfB_2-rich surface compared to the SiC-rich surface. In comparison, during the oxyacetylene flame testing the HfB_2-rich surface suffered a greater degree of damage during a four minute test than that experienced by the SiC-rich surface. This highlights the significant differences between the results arising from different test methods in which not only temperature but also gas flow rates differ and the effect this has upon the surface reactions and damage. As a result, direct comparisons between different high temperature test methods are rarely meaningful.

Tang et al.[8] prepared a range of UHTC composites using 2D carbon fiber (ex-PAN Toray T700) preforms and five different mixes of aqueous UHTC powder slurries based on ZrB_2, SiC, HfC and TaC. A pressure assisted technique was used to impregnate the powders into the fiber preforms and then pyrolytic carbon deposition was used to hold the powders in place. Analysis showed the UHTC powders to be concentrated in a surface layer no more than ~2 mm deep. The hybrid UHTC composites were tested using an oxyacetylene flame; different gas ratios were used to obtain different temperatures and heat fluxes. At 1800°C and 2380 kW m^{-2} the compositions containing SiC demonstrated the lowest erosion depth. However, at the more aggressive conditions of 2700°C and 3920 kW m^{-2} a C/C-ZrB_2 composite outperformed the other compositions. Recently Zhao et al.[9] prepared 3D Cf-ZrC composites using a precursor impregnation and pyrolysis route, studied the mechanical properties and evaluated the high temperature resistance using an oxyacetylene torch. They reported that the

formation of ZrO_2 melt on the surface contributed to a superior high temperature performance.

The present study is designed to investigate further the potential of carbon fiber based UHTC composites for ultra high temperature applications. A number of UHTC powder compositions were used to prepare composites and the high temperature performance was evaluated using a custom built oxyacetylene torch test facility. The composites were characterized before and after high temperature testing.

Experimental

ZrB_2 (Grade B, 1.5 – 3 µm), SiC (Grade UF-25, 0.45 µm), LaB_6 (Grade C, 2 – 3 µm), HfB_2 (325 mesh, <44 µm) and HfC (325 mesh, <44µm) were procured from H. C. Starck (H. C. Starck GmbH, Goslar, Germany). Prior to further processing, they were characterized using XRD (Bruker D8 diffractometer, Bruker AXS GmbH, Karlsruhe, Germany), FEGSEM (Leo 1530VP FEGSEM, LEO Elektronenskopie GmbH, Oberkochen, Germany), EDS (EDAX, EDAX Inc., NJ, U.S.A.), XPS (ESCALAB 5, VG Scientific, West Sussex, UK), BET (Tristar 3000, Micromeritics Instrument Corporation, Norcross, U.S.A) and particle size analysis (Mastersizer 2000, Malvern Instruments Ltd, Worcestershire, UK). 30 mm dia x 17 mm thick 2.5 D needled Cf preforms with 23 vol% fibers were obtained from Surface Transforms plc., Cheshire, UK, whilst phenolic resin (Cellobond J2027L) with a carbon content of ~45.5% (at 900°C under an inert atmosphere) was obtained from Hexion Specialty Chemicals, B. V., Rotterdam, The

Netherlands. UHTC powder / phenolic resin / acetone slurries were prepared by ball milling the ingredients in a plastic container using alumina milling media for 48 h. A typical slurry composition consisted of 40 g of UHTC powder, 20 g phenolic resin and 12.5 g acetone. 5 different UHTC powder/compositions were used to prepare the slurries including ZrB_2, ZrB_2-20 vol% SiC (ZS20), ZrB_2-20 vol% SiC-10 vol% LaB_6 (ZS20-1La), HfB_2 and HfC.

The Cf preforms obtained from Surface Transforms were impregnated with the prepared slurries using a squeeze impregnation technique where the preforms were fully immersed in a beaker containing the slurry and squeezed manually repeatedly to achieve maximum slurry intake. Four composites were prepared for each composition and the impregnated preforms were dried in an air oven at 75°C for 4 h followed by curing at 150°C for 2 h. This entire cycle was repeated 3 times to maximize the amount of UHTC powder within the composite. After the third impregnation and curing, the samples were pyrolysed at 900°C for 2 h using a tube furnace under flowing argon (99.998% pure) using a heating and cooling rate of 1.5°C min^{-1}. After pyrolysis, a 10 mm dia. x 5 mm deep hole was drilled at the bottom of the composites and further densification was achieved using chemical vapor infiltration (CVI) of carbon at Surface Transforms using a commercial process. Benchmark carbon-carbon (C-C) composites were also prepared by CVI that had not undergone UHTC powder impregnation. The change in mass of the samples was recorded after each stage in the preparation process and the bulk density of the composites was measured geometrically.

Representative composites were mounted in epoxy resin, cross sectioned and polished using a semi-automatic polishing machine (TegraPol-25, Struers Ltd., Solihull, UK) with successively finer diamond polishing discs. The final polish used a 1 µm diamond slurry and the samples were analyzed using SEM (Leo 1530VP FEGSEM, LEO Elektronenskopie GmbH, Oberkochen, Germany) to find the depth of impregnation of the powder into the carbon fibre preform. The powder distribution and the efficiency of powder mixing were evaluated using EDS mapping (EDAX, EDAX Inc., NJ, U.S.A.). After CVI, the samples were analyzed using micro-CT (Metris X-Tek 160Xi, X-Tek Systems Ltd., Hertfordshire, UK) to determine again the depth of impregnation and the distribution of UHTC powder within the Cf preform.

The high temperature oxidation performance of the UHTC composites was studied along with the benchmark carbon-carbon composites utilizing a custom built oxyacetylene torch test rig, shown in Figure 1, with an oxygen rich flame (1:1.35 acetylene to oxygen ratio). The specimens were fixed in a water cooled graphite sample holder with three graphite bolts and a K type thermocouple, connected to a data logger, was placed in contact with the back face of the sample through a hole drilled in the sample holder to record the local temperature. The front face temperature was recorded using a 2 color pyrometer (Marathon MR1SCSF, Raytek GmbH, Berlin, Germany) and the temperature distribution was recorded using a modified infrared thermal imaging camera (Thermovision A40 FLIR Systems AB, Danderyd, Sweden). The 2 color pyrometer was capable of recording temperatures from 1000° to 3000°C and the modified thermal imaging camera could record temperatures up to 2800°C when

combined with the neutral density filter.[2] The aim of the preliminary testing was to rank the UHTC composites according to their oxidation performance and hence the tests were carried out for 30 s and 60 s. The mass loss of the samples after oxyacetylene torch testing was recorded and the depth of erosion was determined from micro-CT images. The oxidation products were characterized using FEGSEM, EDS, XRD and micro-CT.

Results and Discussion

The mass of the Cf preforms before impregnation and the mass and bulk density of the composites after impregnation and CVI are summarized in Table 1. The mass increase for the two Hf - based compositions was proportionately lower than for the ZrB_2 - based compositions, given that the density of the former is higher. This was due to the larger particle size of the Hf - based powders (<44 μm) compared to ZrB_2 (1.5 – 3 μm), which limited penetration into the carbon fiber preform.

Figure 2a shows a cross-sectional analysis of one of the composites. 15 Cf layers with alternating fiber orientation (0/90) can be distinguished within the composite and the UHTC powder penetrated from one side of the preform to the other. From the higher magnification images of the outermost layers, figure 2b and c, it can be observed that these layers are somewhat denser as they are rich with UHTC powder, which is ideal for the potential to offer better oxidation and erosion resistance. The level of powder impregnation achieved with the pressureless slurry impregnation technique was better

than that achieved by Tang et al.;[8] they reported a dense outer layer thickness of just 0.75 mm, even with a pressure assisted technique. This could be due to a difference in viscosity between the slurries, differences in UHTC powder particle size or differences in porosity between the preforms; none of these parameters were reported previously.[8]

The depth of impregnation was further analyzed on carbon CVI densified composites using micro-CT and a representative image is shown in Figure 3. The 10 mm dia x 5 mm deep hole drilled into the back face of the sample to facilitate the CVI is also clearly distinguishable. The brighter areas indicate the presence of UHTC powder; it is very evident that the UHTC powder has penetrated very well into the preform with the depth of impregnation being ~7 mm.

In addition to the depth of impregnation, a good powder distribution is also important to achieve superior high temperature performance. Figure 4 shows the EDS mapping on the cross section of a Cf-ZS20 composite. This image shows that good powder mixing was achieved after ball milling, leading to a uniform distribution of the UHTC powder constituents within the preform.

The time-temperature plots for the UHTC composites tested for 30 s using the oxyacetylene torch are presented in Figure 5. The composites were introduced into the flame by manually moving the sample stage, a process that took ~2 s. As the 2 color pyrometer can only record the temperature above 1000°C, the moment at which this first reading was recorded on the pyrometer was taken as ‘zero time’ when plotting the

time-temperature graphs. This, along with the manual monitoring of test duration resulted in slight differences in the total test duration (1-2 s). From the graph it can be seen that the temperature increased at a rate of ~500°C s^{-1} to ~2200°C and then continued to increase slowly for all the samples, except for the C-C sample where the recorded temperature was much lower than that of all other samples. The initial cooling rate was ~1000°C s^{-1} and all the composites survived the high heating/cooling rates.

The time-temperature plot for the samples tested for 60 s is shown in Figure 6. Two C-C samples were tested at this temperature and as for the 30 s test, the recorded temperatures were much lower for the C-C samples even though the same gas flow rates were used for testing all the samples. This is believed to be due to the absorption of some of the heat by the carbon matrix during ablation.[10]

Photographic images of the various composites after 30 s oxyacetylene torch testing are shown in Figure 7. Whilst the effects of oxidation are clear, no appreciable erosion was observed for any of the UHTC-based samples, even though cracking was visible on the front face. An interesting feature observed for the Cf-HfC composite is the lack of adhesion of the oxide layer that formed to the base composite; it fell off during cooling. The main reasons for this is believed to be the build-up of pressure below the oxide layer due to CO/CO_2 gas formation and the absence of formation of any glassy phases during the test.

Figure 8 shows the images of the composites after 60 s of oxyacetylene torch testing whilst Figure 9 shows the 2D micro-CT images highlighting the depth of erosion. Table 2 summarizes the peak front and back face temperature, mass loss data and erosion depth after the 30 and 60 s oxyacetylene torch tests; note that the Cf-HfC sample was analyzed after the surface oxide layer had dropped off. The depth of erosion was found to be the lowest for the Cf-HfB_2 system. From Figure 8, it can be observed that the C-C sample was eroded over a 20 mm diameter area on the front face of the sample and the depth of erosion was measured to be ~4 mm. The surface erosion of the Cf-ZrB_2 and Cf-ZS20 composites were similar to each other, with the damage mainly focused over an area of ~5 mm in diameter and the depth of erosion was 4.8 mm and 5.3 mm respectively. In the case of Cf-ZS20-1La composite, the high temperature flame penetrated through the dense UHTC powder rich layer attacking the C-C layer below, resulting in increased erosion to a depth of ~6.2 mm. The extent of damage was observed to be much lower for the preforms impregnated with either HfB_2 or HfC. The surface oxide layer formed on the Cf-HfC sample detached within a few minutes of extinguishing the flame. The presence of molten phases can be seen on the HfB_2 and HfC-based composites. On visual inspection, the amount of melting was much lower than that for the ZrB_2-based composites, Figure 8, because of the higher melting temperature of HfO_2 (reported to be as high as 2900°C[11] compared to 2715°C for ZrO_2.[12])

It is not entirely valid to make a direct comparison between the measured back face temperatures as the distances between the front face of the samples, where the flame

was focused, and the position where the thermocouple was placed were not the same for all the samples. Also the distance between the flame and the thermocouple changed with time as the high temperature flame eroded the composite.

The reactions schemes for the oxidation of the various UHTC constituents used in the composites are given below.

$$ZrB_2\,(s) + \frac{5}{2}O_2 \rightarrow ZrO_2\,(s) + B_2O_3(l) \qquad \textit{Eqn..(1)}$$

$$B_2O_3\,(l) \rightarrow B_2O_3\,(g) \qquad \textit{Eqn..(2)}$$

$$SiC\,(s) + \frac{3}{2}O_2\,(g) \rightarrow SiO_2\,(l) + CO\,(g)\,(passive) \qquad \textit{Eqn..(3)}$$

$$SiO_2\,(l) \rightarrow SiO_2\,(g) \qquad \textit{Eqn..(4)}$$

$$SiC\,(s) + O_2\,(g) \rightarrow SiO\,(g) + CO\,(g)\,(active) \qquad \textit{Eqn..(5)}$$

$$LaB_6\,(s) + \frac{21}{4}O_2\,(g) \rightarrow \frac{1}{2}La_2O_3\,(s) + 3B_2O_3\,(l) \qquad \textit{Eqn..(6)}$$

$$La_2O_3\,(s) + ZrO_2\,(s) \rightarrow La_2Zr_2O_7\,(s) \qquad \textit{Eqn..(7)}$$

$$HfB_2\,(s) + \frac{5}{2}O_2\,(g) \rightarrow HfO_2\,(s) + B_2O_3\,(l) \qquad \textit{Eqn..(8)}$$

$$HfC\,(s) + \frac{3}{2}O_2\,(s) \rightarrow HfO_2\,(s) + CO\,(g) \qquad \textit{Eqn..(9)}$$

The reaction products formed after the high temperature testing were characterized using XRD as shown in Figure 10 and the results revealed that the surface layer contained only monoclinic-zirconia (m-ZrO_2) for all the ZrB_2 containing UHTC composites and monoclinic hafnia (m-HfO_2) for the HfB_2 and HfC containing composites. Of the various reaction products mentioned in the reaction schemes, ZrO_2

and HfO_2 are stable at >2500°C. B_2O_3 has a very low melting point of 450°C and high vapor pressure and hence it will have quickly vaporized at temperatures above 1100°C.[13] This will have generated porosity and have accelerated the oxidation process above this temperature. Addition of SiC can significantly improve the oxidation resistance in the intermediate temperature range from 1200 to ~1700°C by forming an SiO_2 scale which reduces the oxygen diffusivity,[14] but no SiO_2 peaks were observed in the XRD. Above ~1500°C, SiC undergoes active oxidation leading to the formation of SiO and CO without forming a protective silica layer and hence it does not offer any additional protection.[15] Furthermore, the formation of water molecules as a result of the burning of the acetylene gas can reduce the stability of any SiO_2 that does form by generating $Si(OH)_4$, $SiO(OH)_2$ and/or SiO(OH).[16] Addition of LaB_6 to ZrB_2 is reported to stabilize the ZrO_2, formed as a result of the oxidation of ZrB_2, in the tetragonal phase. The formation of $La_2Zr_2O_7$ pyrochlore, which has a high melting point (>2300°C), has also been reported.[16] From the oxidation testing it was found that the addition of LaB_6 actually reduced the high temperature performance of the UHTC composites and XRD analysis did not detect the presence of any $La_2Zr_2O_7$. FEGSEM images of one of the molten droplets formed on the surface of a Cf-ZS20-1La composite showed the formation of platelet-like structures and an EDS spectrum confirmed the presence of La, Zr, and O, Figure 11. So it can be assumed that $La_2Zr_2O_7$ formed during the torch testing, but melted, segregated and recrystallized without offering any additional protection. Addition of lower valence cations such as La^{3+} to ZrB_2 has been reported to increase the oxygen transport through the oxide layer and also to lower the eutectic temperature of the oxide scale leading to accelerated oxidation during high temperature

testing.[17] Based on the torch test and XRD results it can be concluded that the addition of SiC or LaB_6 did not significantly improve the oxidation resistance of UHTC composites when exposed to temperatures >2500°C using the oxyacetylene torch facility.

Many interesting microstructures were developed in the composites as a result of the combination of the high temperature, rapid heating/cooling and thermal gradients during torch testing. The carbon fibers of the C-C composites underwent severe degradation, Figure 12 a and b. The surfaces of the fibers were also oxidized leading to pitting, Figure 12 c and d and this type of fiber degradation has been reported for Cf composites at elevated temperatures.[10,18,19]

The microstructures formed after the oxyacetylene torch testing of the Cf-ZrB_2 composites, Figure 13, revealed that near the edges the UHTC particles formed large agglomerates that were not strongly bonded to one another, Figure 13a. This is because the temperatures experienced by these particles were lower than in the flame tip region. At 1 – 2 mm from the flame tip, Figure 13b, there was good bonding between the particles and signs of necking. This area was porous and many cracks are also visible. At the flame tip boundary, Figure 13c, liquid phases formed and large, ~5 µm, grains may be seen. Figure 13d is a higher magnification image of one of the droplets formed after the test. This also shows signs of fusing between the particles.

The microstructures of the Cf-ZS20and Cf-ZS20-1La composites were more or less similar to those of the Cf-ZrB_2 composites. Two additional features observed on the surface of the Cf-ZS20 composite are shown in Figure 14. The porosity in what had been molten droplets at higher temperature, Figure 14a, is believed to be due to the escape of B_2O_3, SiO and CO/CO_2 gases generated as a result of the oxidation of ZrB_2 and SiC respectively. The formation of glassy microstructures on the surface, Figure 14b, indicated the formation of borosilicate glasses away from the flame tip, where the sample experienced <2000°C.

The microstructure of the Cf-HfB_2 composite subjected to 60 s oxyacetylene torch testing is shown in Figure 15. This composition offered the best high temperature oxidation protection, even though the powder impregnation was not as good as that achieved for the ZrB_2 based composites, as discussed earlier. Figure 15a reveals the presence of what had been molten HfO_2 and Figure 15b reveals fiber degradation that occurred directly below the flame tip. Figure 15c is a high magnification image on one of the frozen droplets and Figure 15d shows a porous microstructure ~1 – 2 mm away from the flame tip. It may be possible to reduce the extent of fiber damage by improving the HfB_2 impregnation and experiments are underway to achieve this. UHTC powder with finer particle sizes are required to improve further the impregnation.

Conclusions

The potential of Cf-UHTC composites for ultra high temperature applications where ablation is also relevant has been assessed in this study by preparing composites utilizing a slurry impregnation and carbon CVI route. Based on the high temperature oxidation testing, it can be concluded that impregnation of Cf preforms with UHTC powders significantly improves the high temperature oxidation resistance of the composites compared to C-C composites. Hf-based UHTC powders offered superior oxidation protection compared to Zr-based compositions, even though less could be impregnated into the preforms due to a larger mean particle size, and the addition of SiC and LaB_6 did not improve the oxidation resistance at the very high temperatures, >2500°C, investigated Of the two Hf-based compounds, HfB_2 composites showed better oxidation performance as the oxidation products were adherent to the base composite. The thermal shock resistance of all the UHTC composites was found to be excellent.

Acknowledgements

The authors thank the UK's Defence Science and Technology Laboratory (DSTL) for providing the financial support for this work under contract number DSTLX-1000015267 as well as the US Air Force Research Laboratory's Materials and Manufacturing Directorate for ongoing collaborations.

References

1. M.M. Opeka, I.G. Talmy and J.A. Zaykoski. "Oxidation-based materials selection for 2000°C + hypersonic aerosurfaces: Theoretical considerations and historical experience," J. Mater. Sci., 39, 5887-904 (2004).
2. A. Paul, D.D. Jayaseelan, S. Venugopal, et al. "UHTC composites for hypersonic applications," Am Ceram Soc Bull, 91, 22-9 (2012).
3. I.G. Talmy, J.A. Zaykoski and M.M. Opeka. "Synthesis, processing and properties of TaC–TaB_2–C ceramics," Journal of the European Ceramic Society, 30, 2253-63 (2010).
4. J. Han, P. Hu, X. Zhang, S. Meng and W. Han. "Oxidation-resistant ZrB_2–SiC composites at 2200°C," Composites Sci. Technol., 68, 799-806 (2008).
5. A. Sayir, "Carbon fiber reinforced hafnium carbide composite," J. Mater. Sci., 39, 5995-6003 (2004).
6. S.R. Levine, E.J. Opila, M.C. Halbig, J.D. Kiser, M. Singh and J.A. Salem. "Evaluation of ultra-high temperature ceramics for aeropropulsion use," Journal of the European Ceramic Society, 22, 2757-67 (2002).
7. S.R. Levine, E.J. Opila, R.C. Robinson and J.A. Lorincz. "Characterization of an Ultra-High Temperature Ceramic Composite," NASA TM-2004-213085, 1-26 (2004).
8. S. Tang, J. Deng, S. Wang, W. Liu and K. Yang. "Ablation behaviors of ultra-high temperature ceramic composites," Materials Science and Engineering: A, 465, 1-7 (2007).

9. D. Zhao, C. Zhang, H. Hu and Y. Zhang. "Preparation and characterization of three-dimensional carbon fiber reinforced zirconium carbide composite by precursor infiltration and pyrolysis process," Ceram. Int., 37, 2089-93 (2011).
10. D. Cho and B. Il Yoon. "Microstructural interpretation of the effect of various matrices on the ablation properties of carbon-fiber-reinforced composites," Composites Sci. Technol., 61, 271-80 (2001).
11. R. Ruh, H.J. Garrett, R.F. Domagala and N.M. Tallan. "The Systern zirconia-hafnia," J Am Ceram Soc, 51, 23-8 (1968).
12. J. Hlavac, "Melting temperatures of refractory oxides : Part I," Pure & Appl. Chem., 54, 681-8 (1982).
13. W.C. Tripp and H.C. Graham. "Thermogravimetric study of the oxidation of ZrB_2 in the temperature range of 800° to 1500°C," J. Electrochem. Soc., 118, 1195-9 (1971).
14. F. Monteverde and A. Bellosi. "The resistance to oxidation of an HfB_2–SiC composite," Journal of the European Ceramic Society, 25, 1025-31 (2005).
15. W.L. Vaughn and H.G. Maahs. "Active-to-passive transition in the oxidation of silicon carbide and silicon nitride in air," J Am Ceram Soc, 73, 1540-3 (1990).
16. X. Zhang, P. Hu, J. Han, L. Xu and S. Meng. "The addition of lanthanum hexaboride to zirconium diboride for improved oxidation resistance," Scr. Mater., 57, 1036-9 (2007).
17. P. Hu, X. Zhang, J. Han, X. Luo and S. Du. "Effect of various additives on the oxidation behavior of ZrB_2-based ultra-high-temperature ceramics at 1800°C," J Am Ceram Soc, 93, 345-9 (2010).

18. D. Cho, J.Y. Lee and B.I. Yoon. "Microscopic observations of the ablation behaviours of carbon fibre/phenolic composites," J. Mater. Sci. Lett., 12, 1894-6 (1993).

19. W. Han, P. Hu, X. Zhang, J. Han and S. Meng. "High-temperature oxidation at 1900°C of ZrB_2-xSiC Ultrahigh-Temperature Ceramic Composites," J Am Ceram Soc, 91, 3328-34 (2008).

Tables

Table 1 Mass and density of UHTC powder impregnated composites.

Composite	Average mass of carbon fiber preform / g		Final bulk density / g cm^{-3}
	Initial	After UHTC powder impregnation and CVI	
C-C	7.0	26.2	1.86 ± 0.01
Cf-ZrB_2	6.9	29.9	2.11 ± 0.01
Cf-ZS20	6.9	28.8	2.01 ± 0.03
Cf-ZS20-1La	6.8	26.7	1.91 ± 0.03

Cf-HfB_2	7.0	29.3	1.93 ± 0.03
Cf-HfC	7.0	30.3	2.07 ± 0.04

Table 2 Summary of the results after 30 s and 60 s oxyacetylene torch testing

Composite	Test Duration / s	Peak temperature / °C		Weight loss / g	Erosion depth / mm
		Front face (±150°C)	Back face (±10°C)		
CC	30	2210	447	0.38	1.0
Cf-ZrB_2	30	2560	491*	0.22	Negligible
Cf-ZS20	30	2520	477*	0.18	Negligible
Cf-ZS20-1La	30	2575	582*	0.17	Negligible
Cf-HfB_2	30	2625	548*	0.77**	Negligible
Cf-HfC	30	2680	530*	0.55**	Negligible
CC	60	2315	763	1.63	4.0
Cf-ZrB_2	60	2590	857*	0.67	4.8
Cf-ZS20	60	2550	723*	0.63	5.3
Cf-ZS20-1La	60	2525	877*	0.74	6.2
Cf-HfB_2	60	2640	918*	0.57	<2.0
Cf-HfC	60	2530	847*	1.69#	NM

* Back face thermocouple placed inside the drilled hole

** Some of the oxide layer fell off during the test

Includes weight of the lost surface layer

NM Not measured as the surface layer fell off

Figure Captions

Figure 1 Oxyacetylene torch test rig. (1) back face thermocouple, (2) water cooling, (3) sample holder, (4) sample, (5) sample guide, (6) protective insulation, (7) oxyacetylene torch (8) neutral density filter, (9) thermal imaging camera and (10) 2 color pyrometer.

Figure 2 a) Powder distributions across the cross section of a UHTC sample and b) the top and c) bottom layers at higher magnifications.

Figure 3 2D micro-CT images of Cf-ZrB_2 after impregnation and CVI.

Figure 4 FEGSEM image and EDS mapping on the cross section of a Cf-ZS20 composite showing the powder distribution. Carbon (red), silicon (blue) and zirconium (green).

Figure 5 Time-temperature plot for the C-C and UHTC composites tested for 30 s.

Figure 6 Time-temperature plot for the C-C and UHTC composites tested for 60 s.

Figure 7 Photographs of C-C and Cf-UHTC powder composites after 30 s oxyacetylene torch testing. The diameter of the composites was 30 mm.

Figure 8 Photographs of C-C and Cf-UHTC powder composites after 60s oxyacetylene torch test. The diameter of the composites was 30 mm.

Figure 9 Micro-CT images of C-C and Cf-UHTC composites after 60 s oxyacetylene torch test. The images were taken where the depth of erosion was maximum.

Figure 10 XRD analysis of the oxidation products after 60 s oxyacetylene torch testing. All the peaks for the ZrB_2 containing compositions correspond to monoclinic zirconia and the all the peaks corresponding to HfB_2 and HfC containing compositions correspond to monoclinic hafnia.

Figure 11 FEGSEM images and EDS patterns on the molten products formed on the surface of Cf-ZS20-1La composite after torch testing.

Figure 12 Degradation of carbon fiber after the oxyacetylene torch testing of the C-C composites.

Figure 13 Microstructures after 60 s oxyacetylene torch testing of a Cf-ZrB_2 composite a) near the edge of the composite b) 1-2 mm from flame tip c) frozen droplets which had been molten during the test and d) high magnification on one of the frozen droplets.

Figure 14 Microstructure after oxyacetylene torch testing of a Cf-ZS20 composite. a) Porosity observed on the frozen droplets which had been molten at the test temperature and b) glassy structure formed on the composite ~10 mm from the flame tip.

Figure 15 Damage to the Cf-HfB_2 composite after 60 s oxyacetylene torch testing. a) Frozen droplets of HfO_2, b) fiber degradation directly below flame tip c) higher magnification on the frozen droplets and d) porous microstructure.

UHTC Composites: Preparation, Oxyacetylene Torch Testing and Characterization

Figures

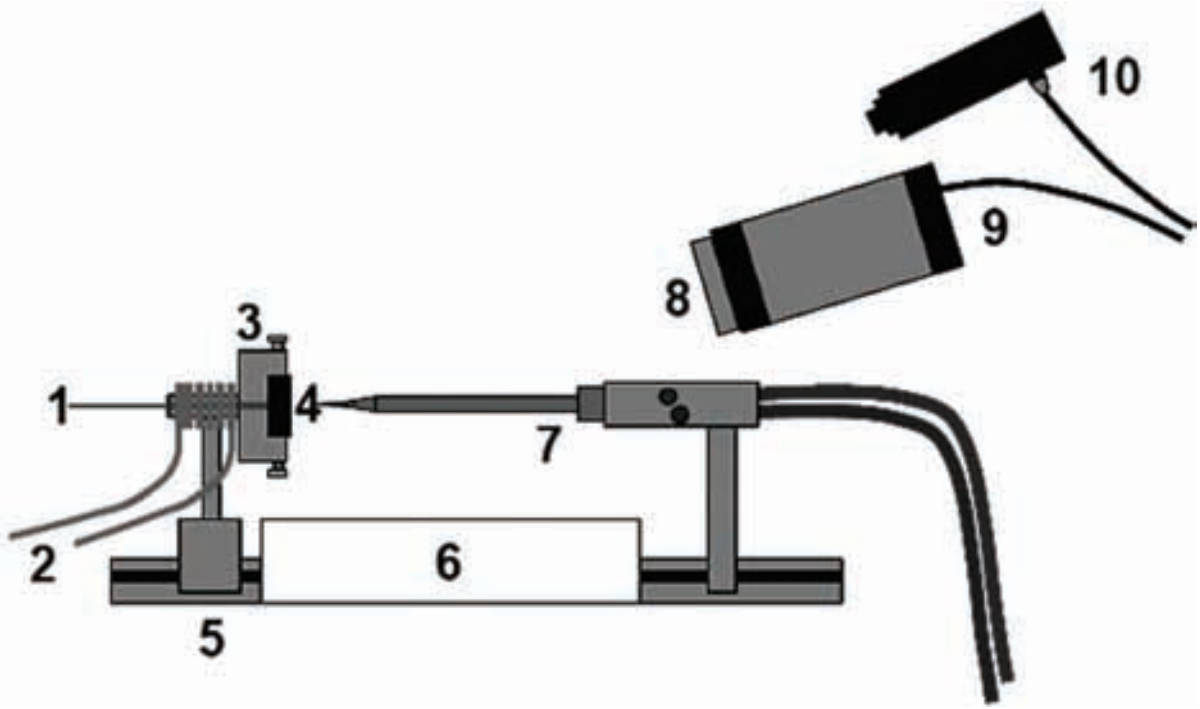

Figure 1 Oxyacetylene torch test rig. (1) back face thermocouple, (2) water cooling, (3) sample holder, (4) sample, (5) sample guide, (6) protective insulation, (7) oxyacetylene torch (8) neutral density filter, (9) thermal imaging camera and (10) 2 color pyrometer.

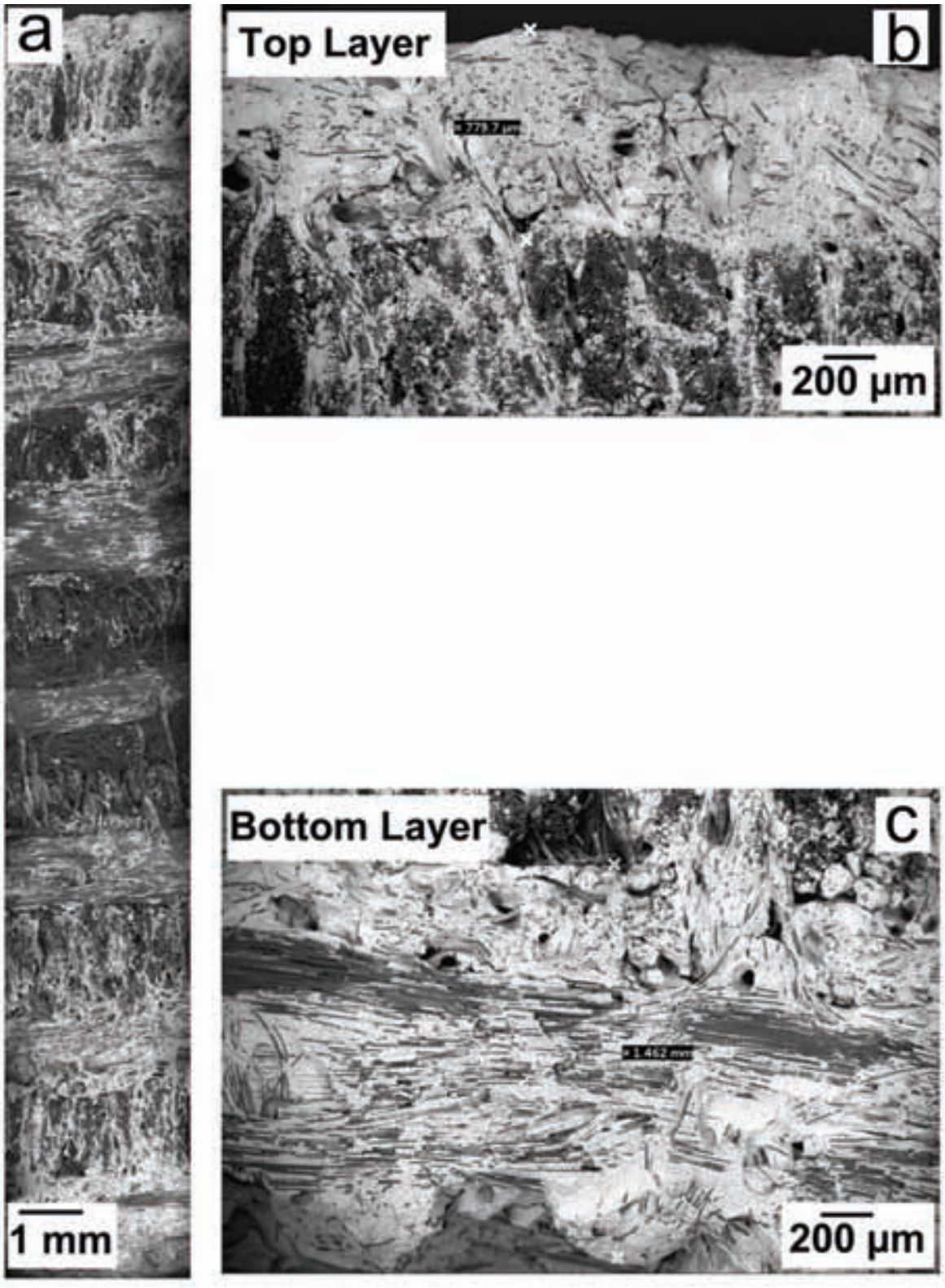
a
1 mm
Top Layer
b
200 µm
Bottom Layer
C
200 µm

Figure 2 a) Powder distributions across the cross section of a UHTC sample and b) the top and c) bottom layers at higher magnifications.

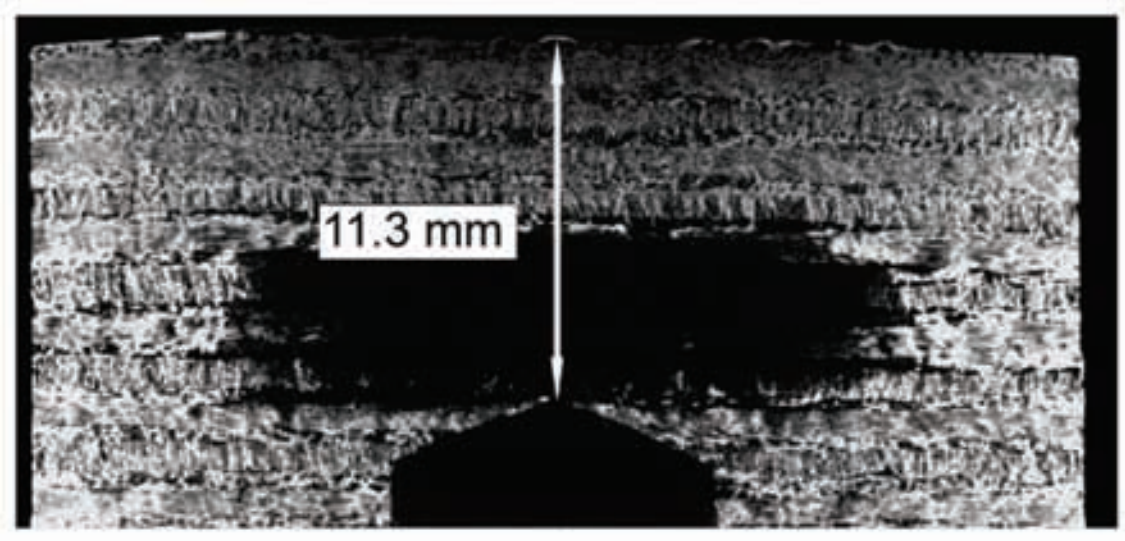

Figure 3 2D micro-CT images of Cf-ZrB_2 after impregnation and CVI.

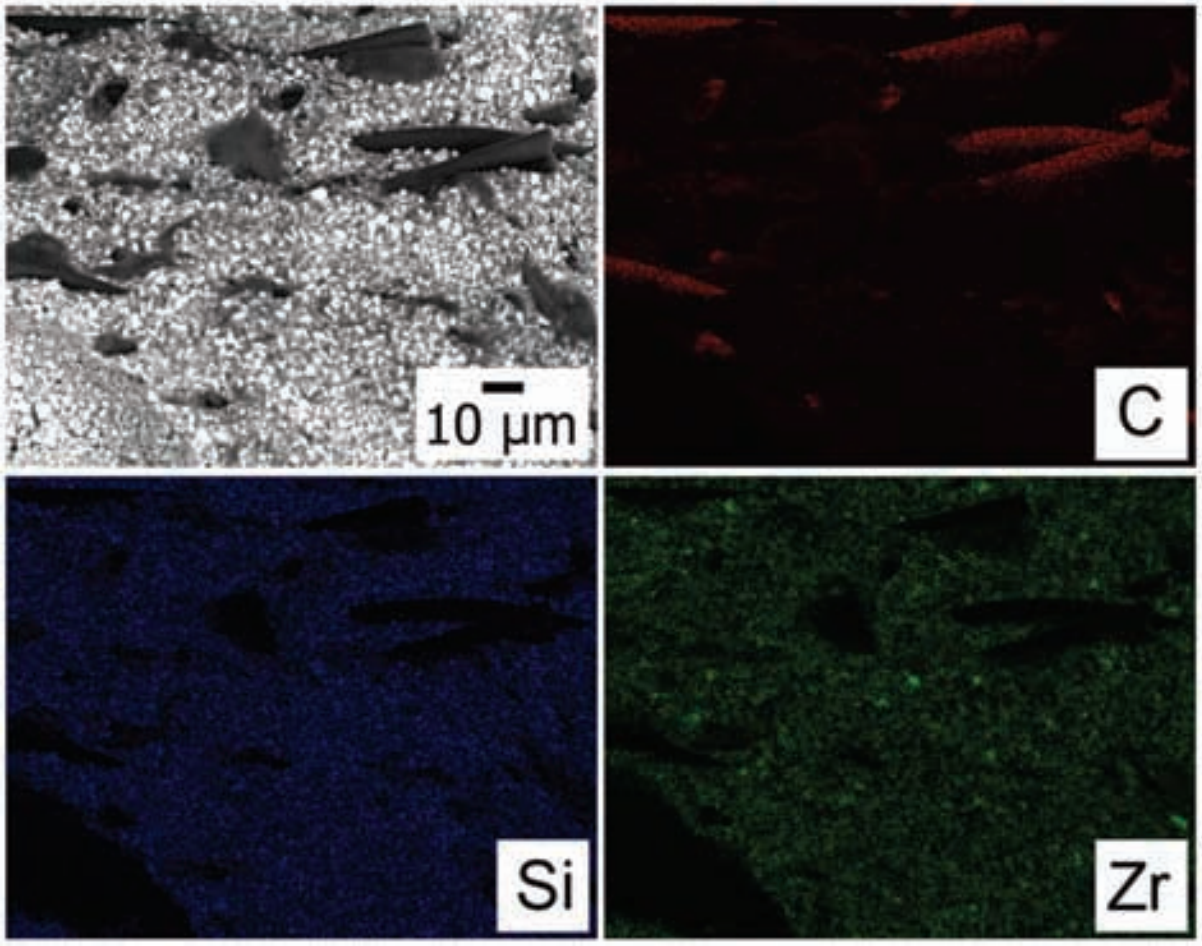

Figure 4 FEGSEM image and EDS mapping on the cross section of a Cf-ZS20 composite showing the powder distribution. Carbon (red), silicon (blue) and zirconium (green).

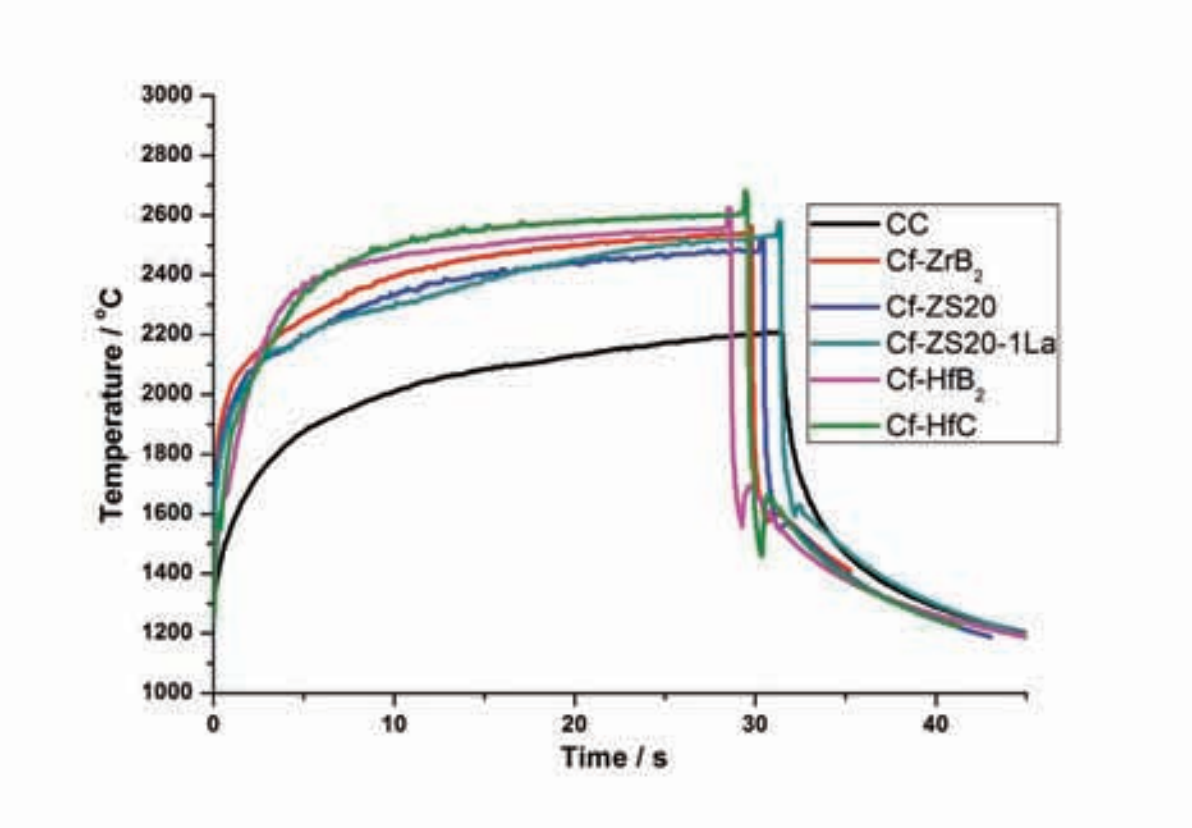

Figure 5 Time-temperature plot for the C-C and UHTC composites tested for 30 s.

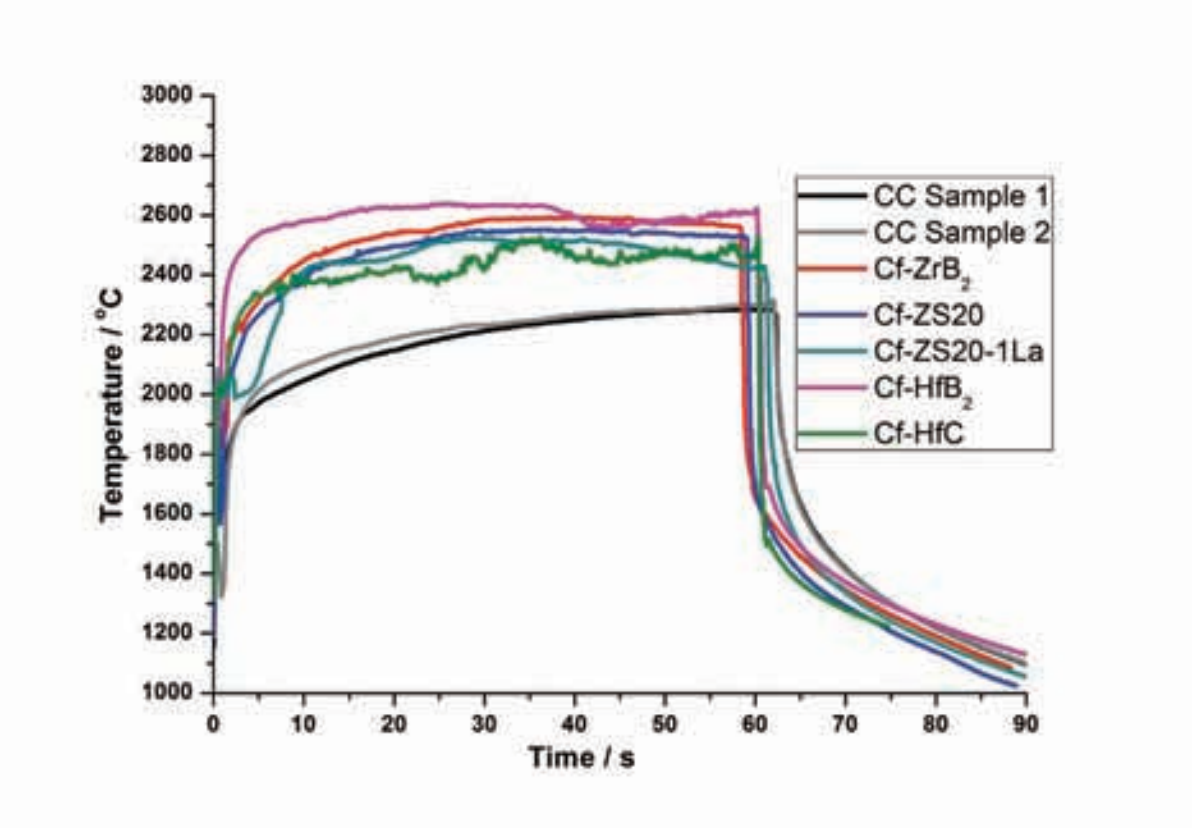

Figure 6 Time-temperature plot for the C-C and UHTC composites tested for 60 s.

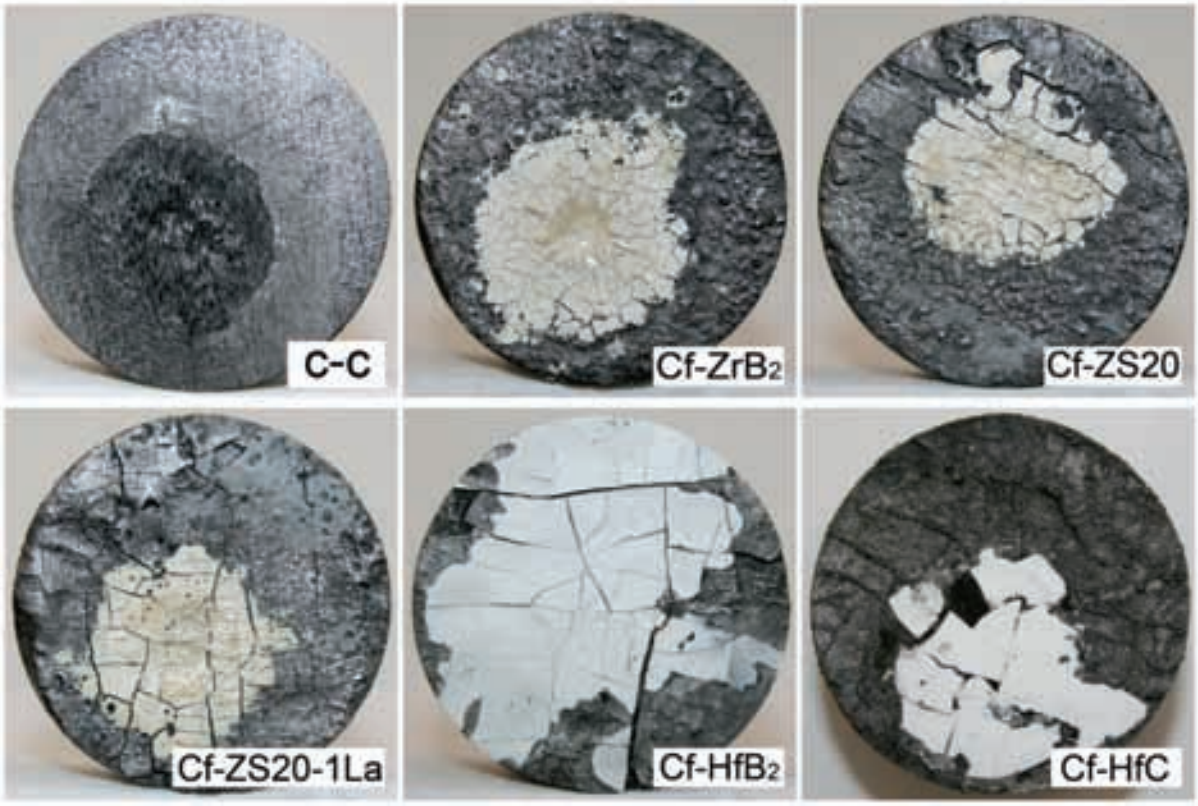

Figure 7 Photographs of C-C and Cf-UHTC powder composites after 30 s oxyacetylene torch testing. The diameter of the composites was 30 mm.

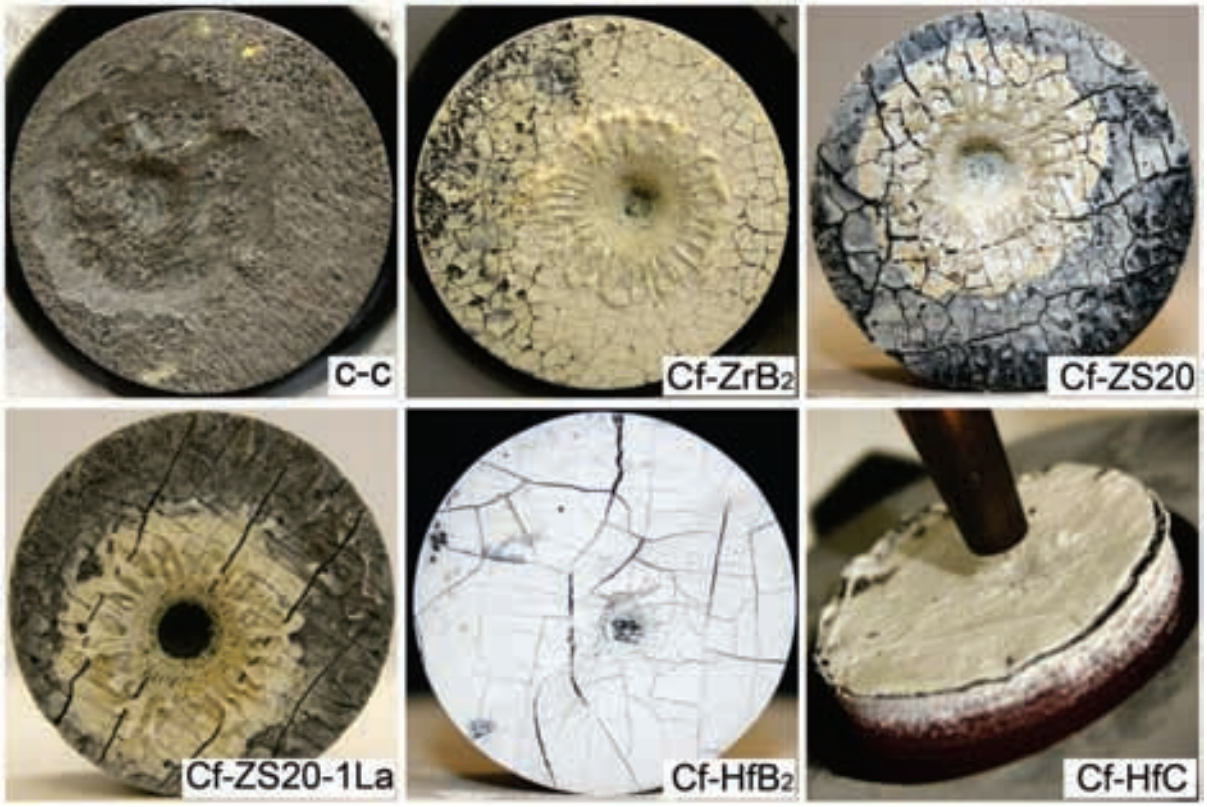

Figure 8 Photographs of C-C and Cf-UHTC powder composites after 60s oxyacetylene torch test. The diameter of the composites was 30 mm.

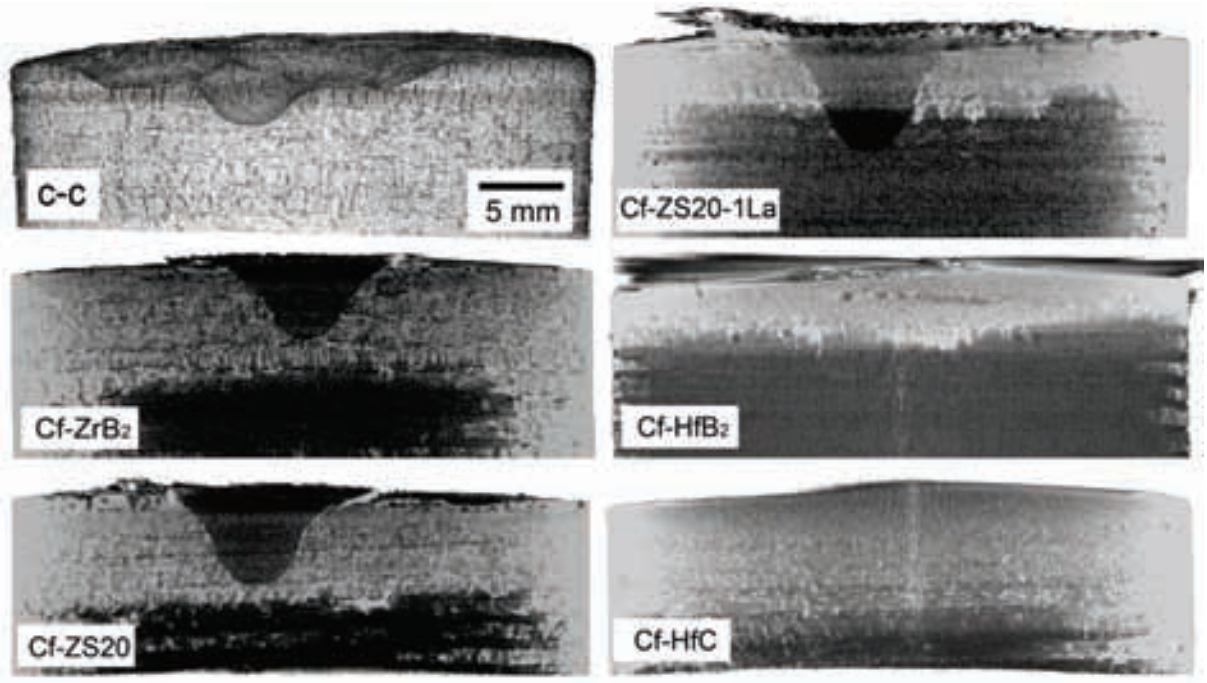

Figure 9 Micro-CT images of C-C and Cf-UHTC composites after 60 s oxyacetylene torch test. The images were taken where the depth of erosion was maximum.

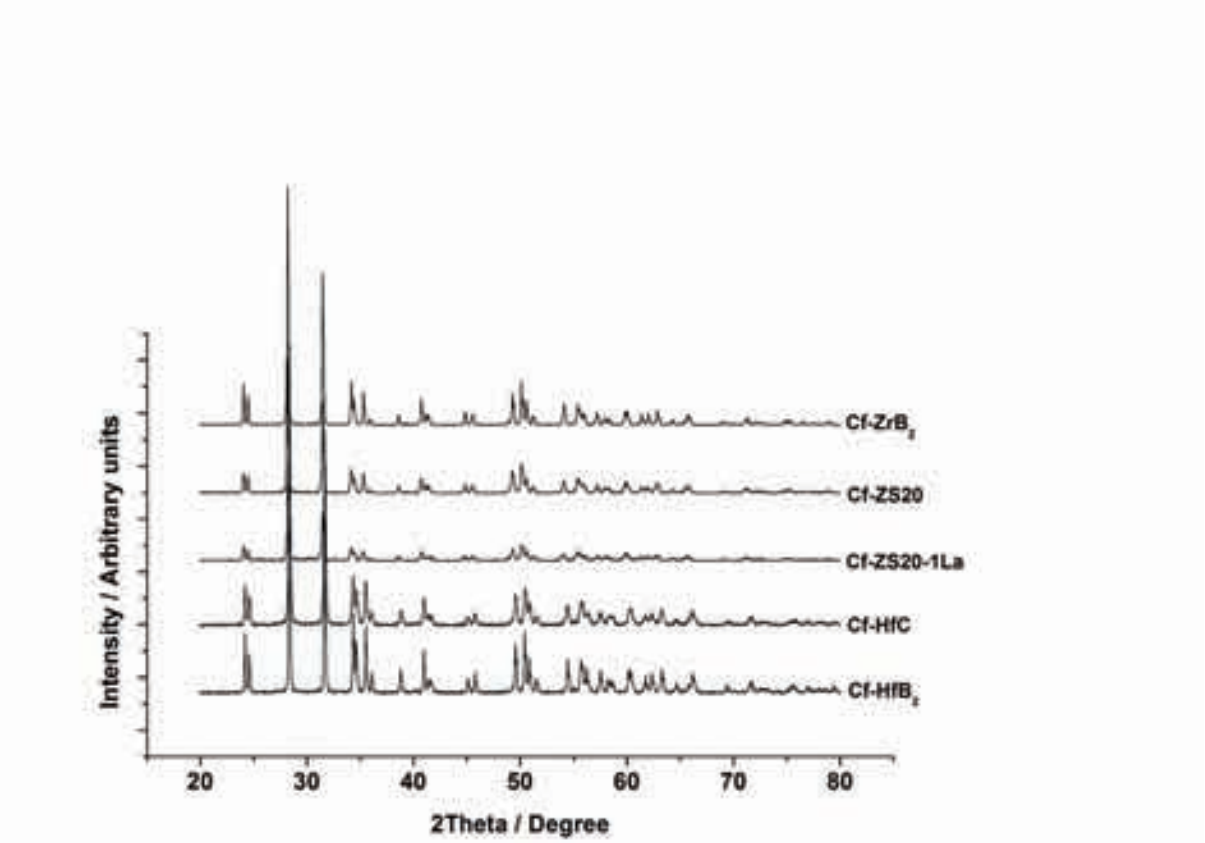

Figure 10 XRD analysis of the oxidation products after 60 s oxyacetylene torch testing. All the peaks for the ZrB_2 containing compositions correspond to monoclinic zirconia and the all the peaks corresponding to HfB_2 and HfC containing compositions correspond to monoclinic hafnia.

Figure 11 FEGSEM images and EDS patterns on the molten products formed on the surface of Cf-ZS20-1La composite after torch testing.

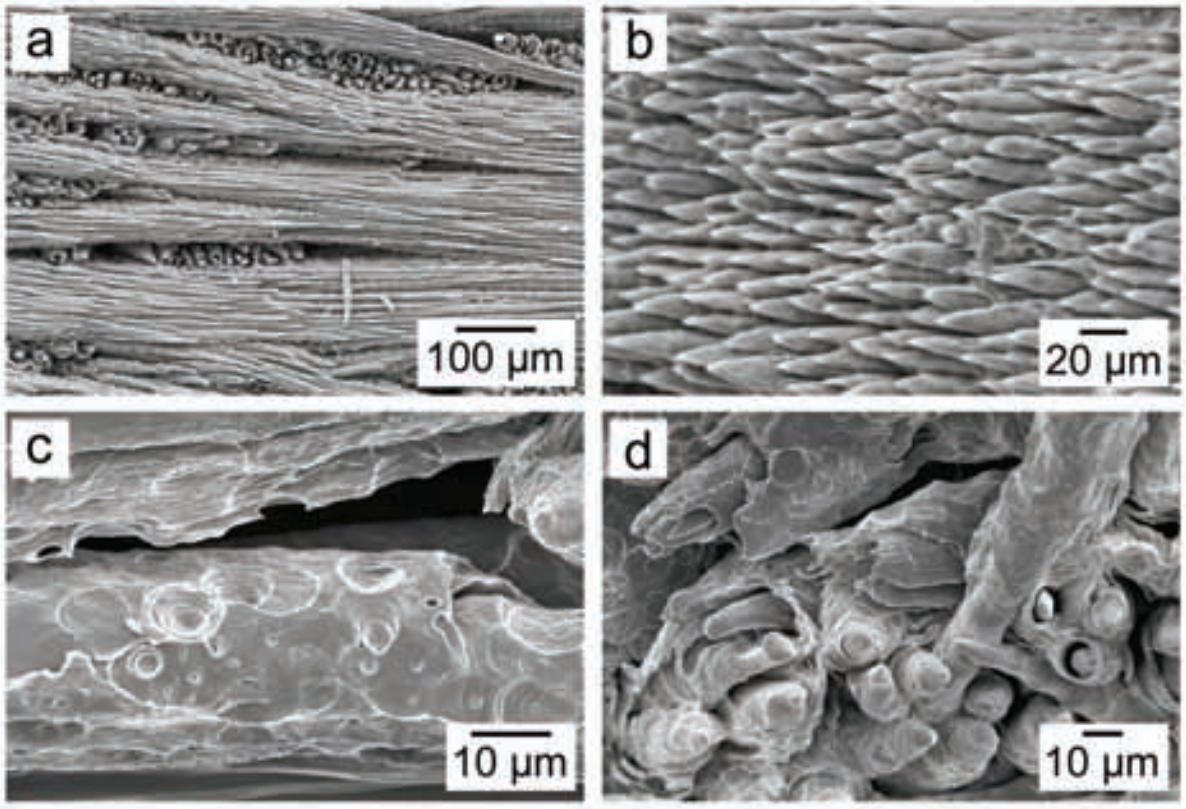

Figure 12 Degradation of carbon fiber after the oxyacetylene torch testing of the C-C composites.

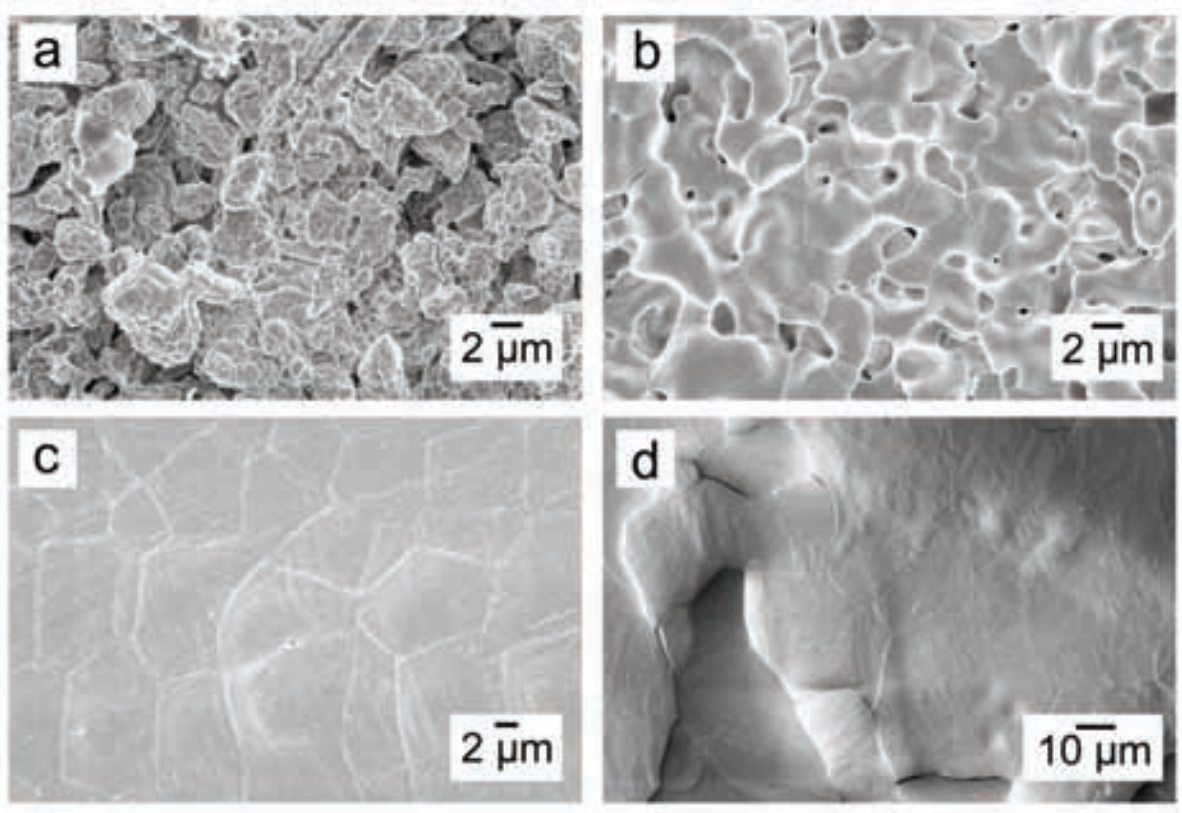

Figure 13 Microstructures after 60 s oxyacetylene torch testing of a Cf-ZrB_2 composite a) near the edge of the composite b) 1-2 mm from flame tip c) frozen droplets which had been molten during the test and d) high magnification on one of the frozen droplets.

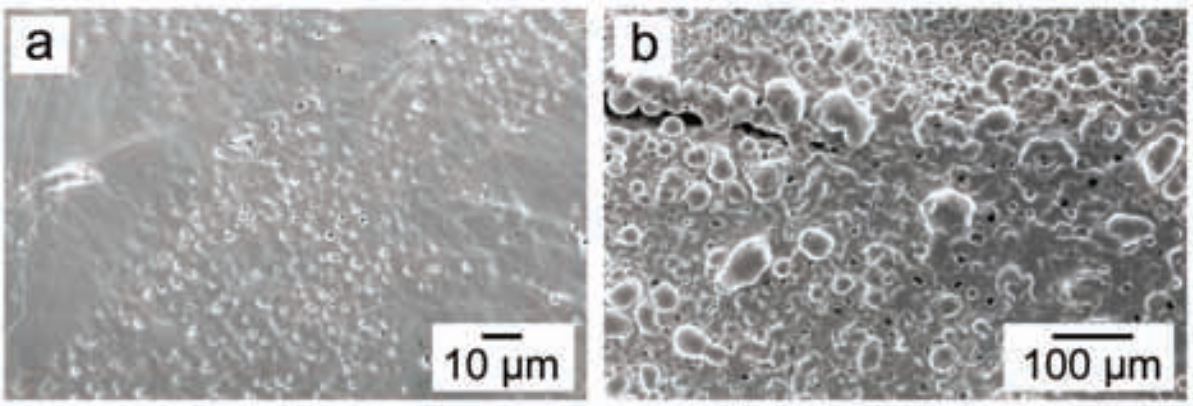

Figure 14 Microstructure after oxyacetylene torch testing of a Cf-ZS20 composite. a) Porosity observed on the frozen droplets which had been molten at the test temperature and b) glassy structure formed on the composite ~10 mm from the flame tip.

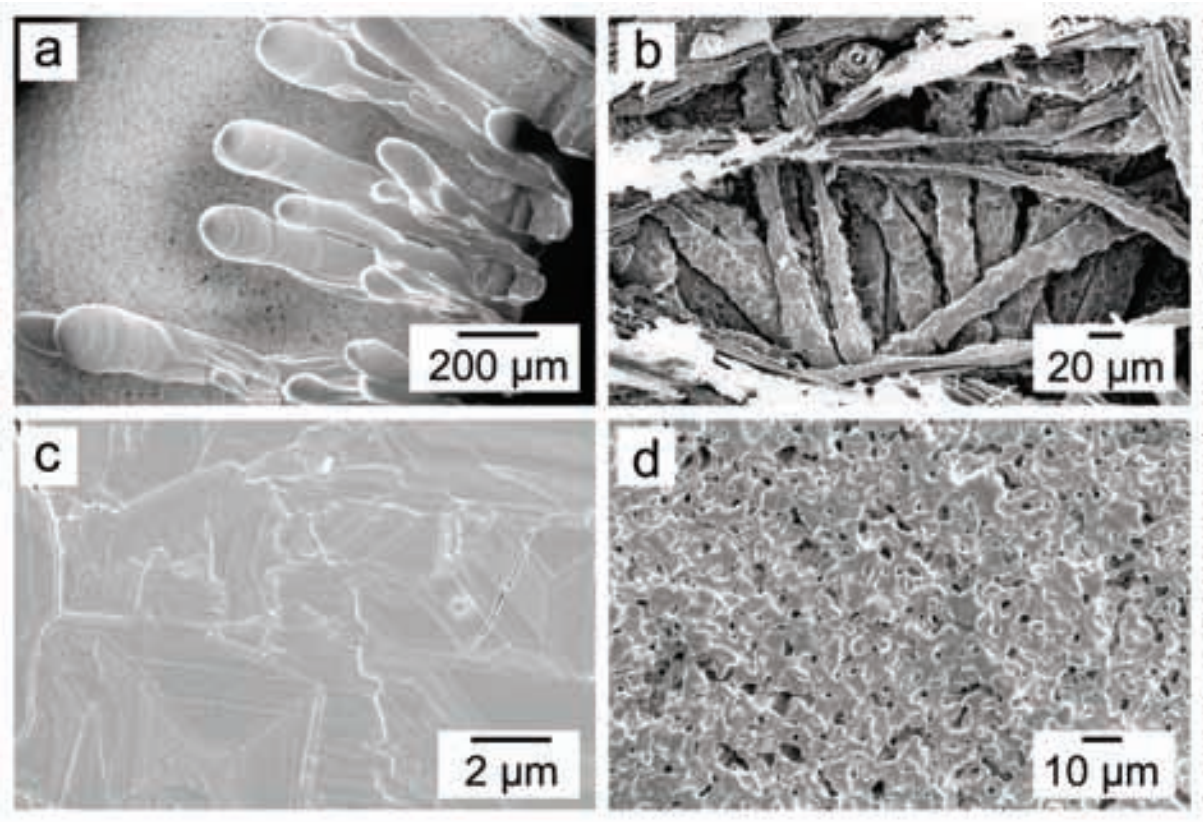

Figure 15 Damage to the Cf-HfB_2 composite after 60 s oxyacetylene torch testing. a) Frozen droplets of HfO_2, b) fiber degradation directly below flame tip c) higher magnification on the frozen droplets and d) porous microstructure.